5

Growth and Characterization of Single Crystals of Potassium Sodium Niobate by Solid State Crystal Growth

Andreja Benčan[1], Elena Tchernychova[1], Hana Uršič[1],
Marija Kosec[1] and John Fisher[2]
[1]*Electronic Ceramics Department, Jožef Stefan Institute,*
[2]*School of Materials Science and Engineering, Chonnam National University,*
[1]*Slovenia*
[2]*Korea*

1. Introduction

Due to the toxic nature of PbO in $Pb(Zr,Ti)O_3$ (PZT), the most common type of piezoceramic, many studies on lead-free materials are being conducted worldwide (Röedel et al., 2009). One of the most studied groups of lead-free ferroelectric materials is based on a solid solution of potassium sodium niobate, $K_{0.5}Na_{0.5}NbO_3$ (KNN) (Jaffe et al., 1971; Kosec et al., 2008). However, activity in attempts to find a lead-free replacement for PZT really accelerated with the discovery of textured $(K,Na,Li)(Nb,Ta,Sb)O_3$ ceramics, with properties comparable to those of PZT (d_{33}> 300 pC/N, relative permittivity > 1500, planar coupling coefficient k_p> 60%)(Saito et al., 2004).

One way to enhance the piezoelectric properties of KNN is to grow KNN-based single crystals along certain crystallographic directions, as has been demonstrated for the case of $KNbO_3$ (Wada et al., 2004) and relaxor-based ferroelectric single crystals (Park & Shrout, 1997). The most frequently used methods for growing alkali niobate based single crystals are top seeded solution growth and the flux methods (Chen et al. , 2007; Davis et al., 2007; Kizaki et al., 2007; Lin et al., 2009). However, these methods are not yet fully commercialized due to high costs and poor reproducibility related to compositional inhomogeneity within the crystals. A possible way to improve the homogeneity of crystals with complex composition is to grow them by the low cost Solid State Single Crystal Growth (SSCG) method.

The SSCG method is essentially a form of induced abnormal grain growth, a phenomenon which is very well known in the solid state sintering community. A significant breakthrough in the solid state synthesis of lead-free materials has been achieved in recent years (Kosec at al., 2010; Malič et al., 2008a). However, due to the strongly hygroscopic nature of alkaline carbonates usually used in solid state synthesis, different diffusion rates of involved ionic species during annealing, and the high sublimation rates of the alkaline species at high temperatures (Bomlai et al., 2007; Jenko et al., 2005; Kosec & Kolar, 1975; Malič et al., 2008b), it may be rather difficult to obtain compositionally homogeneous alkali niobate-based single crystals by SSCG.

The chemical homogeneity and porosity, as well as crystal and domain structure of such single crystals strongly affects their ferroelectric behaviour. They depend on many parameters such as the initial growth setup used for SSCG, i.e. the choice of the seed and the presence of a liquid sintering aid, and further growth conditions, such as annealing rate, temperature, pressure etc. In order to be able to understand the composition-property relationship of single crystals their structure and chemical composition has to be accurately determined. This can be achieved using different complementary analytical methods such as optical, scanning and transmission electron microscopes, X-ray diffraction analysis, etc.
The aim of the following chapter is firstly to present basic principles of the SSCG technique and its application to the growth of $K_{0.5}Na_{0.5}NbO_3$ (KNN) and Li,Ta-modified KNN single crystals. Secondly, the use of complementary analytical characterization techniques for obtaining the precise compositional and structural data from the produced crystals and its correlation with the electrical properties will be discussed.

2. Principles of the solid-state crystal growth technique

The SSCG method is a way of growing single crystals from a polycrystalline starting material. In this method, a single crystal (called a seed crystal) is embedded in ceramic powder of the desired crystal composition and pressed. The sample is then sintered and a single crystal with the composition of the ceramic powder grows using the seed crystal as a template (Fig.1). Alternatively, a seed crystal is placed on top of a pre-sintered ceramic sample and annealed (both the faces of the seed crystal and the ceramic that are in contact must be polished). A single crystal then grows downward from the seed crystal into the ceramic.

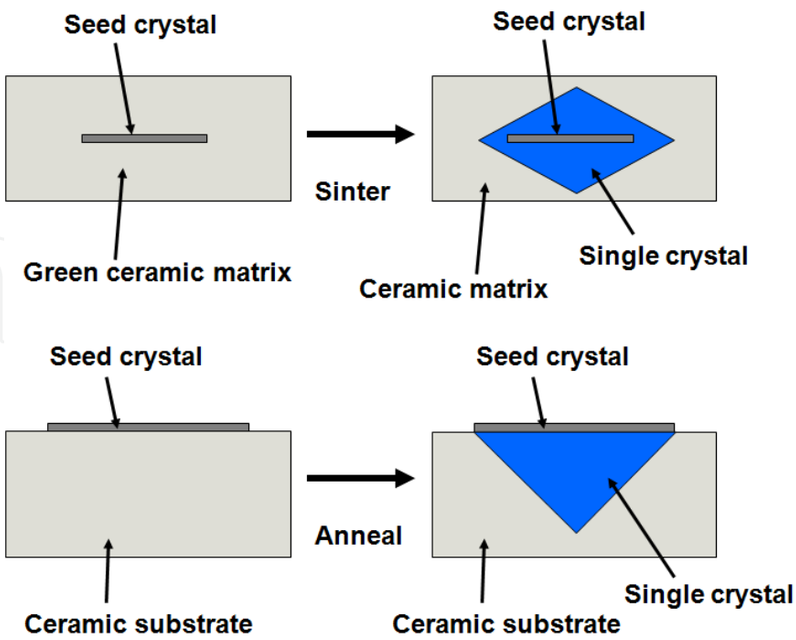

Fig. 1. Schematic of Solid-State Single Crystal Growth

The SSCG method was first used to grow single crystals of $BaTiO_3$ (DeVries, 1964) and has since been used to grow single crystals of manganese zinc ferrite (Kugimiya et al., 1990), $Pb(Mg_{1/3}Nb_{2/3})O_3$–$PbTiO_3$ (Khan et al., 1999), $Pb(Mg_{1/3}Nb_{2/3})O_3$–$PbZrO_3$–$PbTiO_3$ (Zhang et al., 2007), $Ba(Ti,Zr)O_3$ (Rehrig et al., 1999) and $BaTiO_3$ (Yamamoto & Sakuma, 1994). The piezoelectric properties of single crystals grown by the SSCG method are comparable to those of crystals grown by flux-based methods (Lee, 2003).

The SSCG method has several advantages over more traditional flux or melt-based methods of single crystal growth (Lee, 2003). Conventional ceramic processing equipment can be used, avoiding the need for expensive crystal-growing apparatus. The SSCG method is particularly suited to growing single crystals which melt incongruently or which have volatile components. Because the SSCG method does not involve melting and re-solidification of the ceramic powder, problems such as compositional variations in crystals can be avoided. Furthermore, since SSGC is an isothermal crystal growth method, problems of temperature-gradient induced stresses in the crystal are avoided.

However, the SSCG method also has some disadvantages. If pores exist or form in the substrate, they can be included in the growing single crystal (DeVries, 1964; Kim et al., 2006). Once pores are trapped within the crystal they are very difficult to remove, as gases trapped in the pore have to diffuse through the crystal lattice (Choi et al., 2001). Also, if abnormal grain growth takes place in the substrate, these large grains will pin the single crystal boundary, preventing further growth (Kim et al., 2006). So control of the substrate microstructure is vital if good quality single crystals are to be obtained.

The SSGC method utilizes the phenomenon of abnormal grain growth. Abnormal grain growth also frequently occurs in the ceramic matrix/substrate during the sintering/annealing stage. In order to understand and control SSCG, the principles behind abnormal grain growth in ceramics must first be discussed. When a polycrystalline ceramic undergoes abnormal grain growth, a small number of grains (abnormal grains) grow much more rapidly than the other grains (matrix grains). A bimodal microstructure develops, consisting of fine micron-sized matrix grains and a few large abnormal grains, which can be hundreds of microns in diameter. Sometimes, all of the matrix grains are consumed by the abnormal grains, resulting in a coarse microstructure. Examples of systems which display abnormal grain growth include $BaTiO_3$ (Hennings et al., 1987) and $Pb(Mg_{1/3}Nb_{2/3})O_3$–$PbTiO_3$ (Seo & Yoon, 2005).

In a polycrystalline ceramic that is being sintered or annealed, each grain will have its own growth rate $\dot{R}$, given by the equation (Chiang et al., 1997):

$$\dot{R} = 2M_b\Delta\mu \tag{1}$$

where M_b is the interface mobility and $\Delta\mu$ is the driving force for grain growth. The driving force for grain growth of a grain (assuming liquid-phase sintering) is given by (Yoon et al., 2001):

$$\Delta\mu = 2\gamma_{sl}\Omega\left(\frac{1}{\bar{r}} - \frac{1}{r}\right) \tag{2}$$

where γ_{sl} is the solid / liquid interfacial energy, Ω the molar volume of the solid phase, r the grain radius and $\bar{r}$ the radius of a critical grain that neither grows nor shrinks. This is usually considered to be the mean grain radius. For solid-state sintering, γ_{sl} is replaced with the average grain boundary energy γ_{gb}.

Whether a ceramic undergoes abnormal grain growth or not depends upon its interface structure. Interfaces (both grain boundaries and solid/liquid interfaces) can be either rough (disordered) or faceted (ordered) at an atomic level (Hirth & Pound, 1963). If the interfaces are rough, then atom attachment can take place at any point on the growing grain and grain growth is controlled by diffusion of atoms through the liquid phase or across the grain boundary between the shrinking and growing grain. If the interfaces are faceted then attachment of atoms to a grain is energetically unfavourable because a number of broken bonds are formed. After atoms adsorb on the grain surface, they will quickly desorb again unless they can migrate and attach to a low energy site such as the edge of a 2D nucleus. Such a grain can therefore grow by the formation and spread of 2D nuclei on the grain surface. Alternately, if a defect such as a screw dislocation or twin is present, then this can also act as a site for grain growth.

Fig.2 shows the variation of the grain growth rate with driving force for rough and faceted interfaces (Hirth& Pound, 1963). For rough solid/liquid interfaces, interface mobility M_b is constant with $\Delta\mu$ and the growth rate is given by (Greenwood, 1956):

$$\dot{R} = \frac{DC_0\Omega\Delta\mu}{2kTr} \tag{3}$$

where D is the diffusivity of the solid through the liquid phase, C_0 the equilibrium solubility and T the temperature. The growth rate is linearly proportional to the driving force. Grains larger than the mean radius will grow, whilst smaller grains will shrink. For a system with rough solid/liquid interfaces, abnormal grain growth does not occur (Kwon et al., 2000; Lee et al., 2000).

For faceted interfaces, M_b is not constant with $\Delta\mu$. For grain growth caused by 2D nucleation, the growth rate is described by the following equation (van der Eerden, 1993):

$$\dot{R} \cong \nu_{st}\exp\left(\frac{-\pi\Omega\varepsilon^2}{6h\Delta\mu kT}\right) \tag{4}$$

where ν_{st}, ε, and h are the step velocity of the growing nucleus, edge free energy of the nucleus and step height of the nucleus respectively. For low driving forces, the rate at which stable 2D nuclei form is very low. Hence atoms cannot easily attach to the grain and the growth rate is very slow. Above a critical driving force $\Delta\mu_C$, the rate at which stable 2D nuclei form increases exponentially (Hirth& Pound, 1963). Atoms can then easily attach to the grain and grain growth can take place. The grain growth rate therefore varies exponentially with $\Delta\mu$. For $\Delta\mu>\Delta\mu_C$, kinetic roughening takes place: the number of 2D nuclei available for atom attachment on a grain is so large that atoms can easily attach at any point and grain growth is effectively diffusion controlled, as in the case of a rough interface (Kang, 2005). For a system with faceted interfaces, abnormal grain growth can occur. Most of the grains will have $\Delta\mu<\Delta\mu_C$ and will grow very slowly, but a few grains will have $\Delta\mu\geq\Delta\mu_C$ and can grow rapidly to form abnormal grains. This leads to a bimodal microstructure, with large abnormal grains in a matrix of fine grains.

For faceted interfaces, screw dislocations can act as sites for atom attachment and grain growth (Bauser & Strunk, 1982). The growth rate for an interface containing screw dislocations is described by the Burton-Cabrera-Frank theory (Burton et al., 1951). For a

crystal face with a growth spiral, the growth rate increases parabolically with $\Delta\mu$ for $\Delta\mu<\Delta\mu_C$, and linearly for $\Delta\mu>\Delta\mu_C$ (Bennema, 1993).

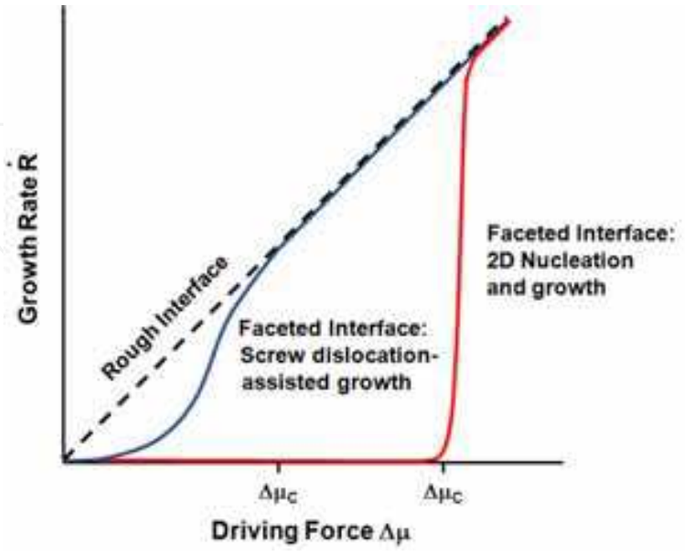

Fig. 2. Variation of growth rate with driving force for rough and faceted interfaces

In the SSCG method, the seed crystal acts as a large grain which can grow abnormally to form a single crystal. Grains in the matrix that are large enough can also undergo abnormal grain growth. For the SSCG method to work, the grains must have faceted interfaces. The seed crystal should have the same crystallographic structure as the desired single crystal, and should have similar unit cell parameters so that epitaxial growth can take place on the seed. In addition, the seed crystal should not react chemically with the matrix material or sintering aid.

3. Characterization methods

Most of the methods that are applicable to the compositional and chemical characterization of bulk ceramics can be employed for the single crystals. One of the most commonly employed methods for exploring ceramic structure is X-ray diffraction (XRD) analysis. Besides crystal structure related analysis, the XRD data gives the information about the bulk phase composition. However, fractions of minor phases below ~3 to ~1 vol%, depending on the XRD configuration, cannot be detected. In case of single crystals, a dedicated XRD setup can be used, if the size of the investigated crystal exceeds 2 mm (Arndt & Willis, 1966).
The microstructure of the material can be explored by the different methods of microscopy, depending on the size of the investigated feature. The optical microscope can be employed for studying larger features and for a general overview of the material. With its specific applications, such as polarization microscopy, the domain structure of the ferroelectric material can be studied with a resolution up to 0.5 μm. Further exploration of the material's microstructure is generally conveyed with a scanning electron microscope (SEM) and a transmission electron microscope (TEM). Here, the local microstructure can be studied at micro- and nano-scales by means of both imaging and electron diffraction. The utilization of the electron back-scattered diffraction (EBSD) technique in SEM allows probing of the

ferroelectric domain structure at the microscale, while the selected area electron diffraction (SAED) patterns obtained in the TEM can be used for studying the nanosized domains.
As well as facillitating the visualization of the microstructure, the electron microscopy techniques make it possible to gain the compositional information from the localized area of the bulk sample. For the bulk material, the complete quantitative elemental composition can be obtained with Inductively Coupled Plasma (ICP) analysis with ppm precision. With energy dispersive X-ray spectroscopy (EDXS) and wavelength dispersive X-ray spectroscopy (WDXS) in SEM it is possible to gain compositional information with micrometer-scale resolution and with typical detection limits of ≈ 0.1wt% and ≈ 0.01 wt.%, respectively (Goldstein et al., 2003). Further improvement of spatial resolution in the compositional analysis can be achieved with TEM-EDXS. Although the detection limits of TEM-EDXS are the same as those in SEM-EDXS, the analyses can be performed with the spatial resolution in the nm range.
It is important to mention that due to the presence of the volatile compounds in alkali based single crystals, the data acquisition and the interpretation of the EDXS analysis have to be performed with caution. Issues such as the spatial resolution, beam-specimen interactions and the use of proper standards should be taken into account to obtain the true chemical composition of KNN single crystals (Benčan et al., 2011). For example, Samardžija et al. (Samardžija et al., 2004) showed that the standardless quantitative EDXS analysis of polycrystalline KNN gave erroneous compositions for the KNN solid solution. Another point which was made by the authors was concerning the proper choice of analytical standards. Glasses containing Na and/or K or natural minerals with Na and/or K (albite, orthoclase) which are usually used as standards in virtual standard packages for standardless SEM-EDXS methods are not reliable enough due to the appearance of compositional variations and the well known beam-induced alkali migration within a single specimen. Additionally, the alkali content in these minerals is rather low, which affects the precision of the analysis. Instead, the use of reliable, homogeneous and stable standard materials such as single crystals of $KNbO_3$ and $NaNbO_3$ is proposed.

4. Growth of $(K_{0.5}Na_{0.5})NbO_3$ single crystals by SSCG.

As was already discussed in Section 2, seed crystals and ceramic powder precursors are needed to grow KNN single crystals by SSCG. For the KNN system, $KTaO_3$ was found to be a suitable material for seed crystals due to the similarity in unit cell parameter between $KTaO_3$ (a=3.9883Å) (ICSD #39673) and $K_{0.5}Na_{0.5}NbO_3$ (a=4.0046Å, b=3.9446Å, c=4.0020Å, and β=90.3327°) (Tellier et al., 2009). Also, $KTaO_3$ does not undergo any phase transitions during cooling which could produce stresses and cracking in the single crystal. For the growth of KNN single crystals, $KTaO_3$ single crystal seeds (FEE GmbH, Germany) oriented in the <001>and <110>directions were used.
The precursor powder with a composition of $(K_{0.5}Na_{0.5})NbO_3$ was prepared by attrition milling K_2CO_3 (Aldrich, 99+%), Na_2CO_3 (Riedel-de Haën, 99.8%) and Nb_2O_5 (H. C. Starck, 99.8%) in acetone with ZrO_2 media, followed by calcination at 700°C for 4 hours. The ceramic powder should have a fine mean particle size and should also have a narrow particle size distribution. The growth rate of the single crystal is inversely proportional to the mean matrix grain size of the ceramic, so a ceramic with a small mean matrix grain size is preferable (Equation 2). To make a precursor ceramic with a small mean matrix grain size, a fine starting powder is necessary. Also, if the starting powder has a wide particle size distribution, the larger particles can grow rapidly to form abnormal grains during sintering

of the ceramic. These abnormal grains will then slow down of even block single crystal growth (Kim et al., 2006).

It may be necessary to add a liquid phase sintering aid to the powder. For the PMN-PT system, addition of PbO as a liquid phase sintering aid increases the growth rate of the single crystal (Gorzkovski et al., 2006). In the experiments described below, $K_4CuNb_8O_{23}$ was used as a liquid phase sintering aid (Matsubara et al., 2005). To make $K_4CuNb_8O_{23}$, K_2CO_3, CuO (Alfa Aesar, 99.7%) and Nb_2O_5 were attrition milled and calcined at 700°C for 4 hours. The effect of $K_4CuNb_8O_{23}$ on single crystal growth of $(K_{0.5}Na_{0.5})NbO_3$ will be discussed in a later Section 4.3.

4.1 Growth of $(K_{0.5}Na_{0.5})NbO_3$ single crystals at atmospheric pressure

$KTaO_3$ seed crystals with the dimensions of 2 mm × 2mm × 0.5 mm were buried in 1.2 g of powder and uniaxially pressed at 100 MPa, followed by cold isostatic pressing at 200 MPa. Samples were sintered in air at 1100°C for 10 h, with heating and cooling rates of 2°C.min^{-1}. A scanning electron microscopy (SEM) micrograph of a vertically-sectioned, polished and thermally etched sample is shown in Fig. 3 (Fisher et al., 2007a). The inset shows the boundary between the single crystal and the matrix. A single-crystal ~160μm thick has grown on the seed crystal. Both the single crystal and the polycrystalline matrix contain large numbers of pores.

Quantitative SEM-EDXS analysis was carried out using single crystals of $KNbO_3$ and $NaNbO_3$ as standards (Samardžija et al., 2004). Analysis shows that both the single crystal and the matrix grains have the composition $(K_{0.5}Na_{0.5})NbO_3$ within the limits of experimental error. Furthermore, the EDXS results show that Ta has not migrated from the seed crystal to the single crystal. High resolution Transmission Electron Microscopy (HRTEM) of the seed/single crystal interface shows that the single crystal grew epitaxially on the seed crystal, as shown by the selected area diffraction pattern of the interface in the inset (Fig. 4).

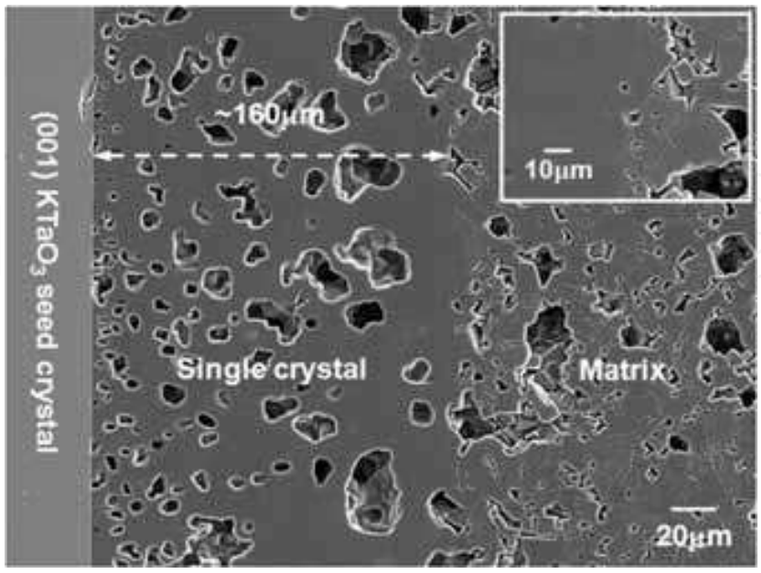

Fig. 3. SEM micrograph of a Single Crystal of $(K_{0.5}Na_{0.5})NbO_3$ grown by SSCG (Fisher et al., 2007a)

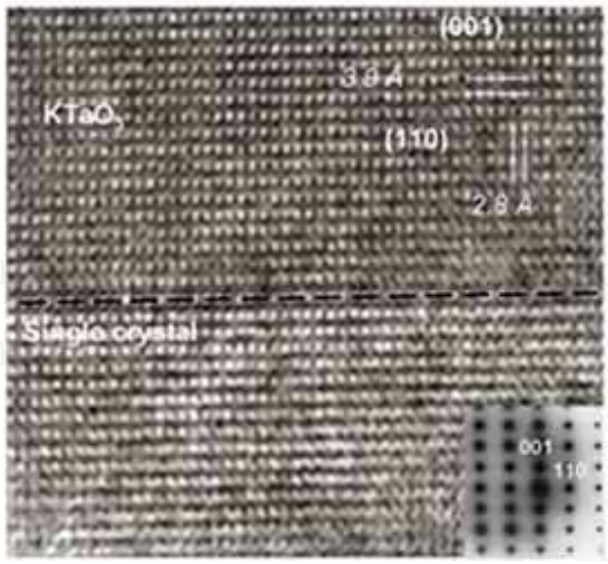

Fig. 4. High resolution TEM (HRTEM) image of the $KTaO_3$ seed crystal / $(K_{0.5}Na_{0.5})NbO_3$ single crystal interface (Fisher et al., 2007a)

4.2 Growth of $(K_{0.5}Na_{0.5})NbO_3$ single crystals in a hot press

As can be seen in Fig. 3 single crystals of $(K_{0.5}Na_{0.5})NbO_3$ grown by the SSCG method are very porous. To solve this problem, single crystals were grown in a hot press (Fisher et al., 2008a). In these experiments, <110>-oriented $KTaO_3$ seed crystals were used.

The sample was pre-densified in the hot press at a temperature of 975°C and a pressure of 50 MPa for 2 h, and then annealed at a temperature of 1100°C and a pressure of 50 MPa for 100 h. In Fig. 5a, the optical micrograph of the resulting single crystal is shown. Compared to a single crystal grown in a conventional box furnace under atmospheric pressure (Fig. 5b), hot pressing made it possible to produce a much denser crystal.

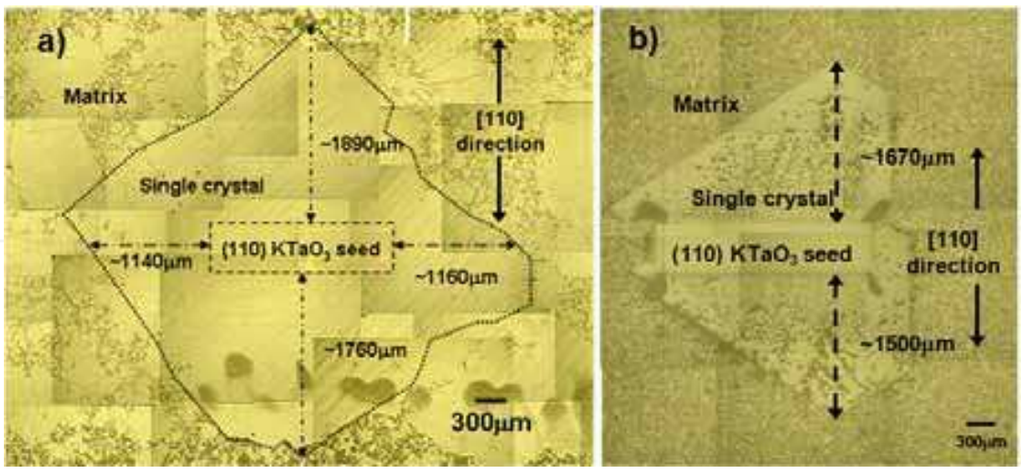

Fig. 5. Comparison of optical micrographs of (a) a $(K_{0.5}Na_{0.5})NbO_3$ single crystal grown in a hot press at 975°C/50 MPa for 2 h, followed by 1100°C/50 MPa for 100 h (b) a $(K_{0.5}Na_{0.5})NbO_3$ single crystal grown in a conventional furnace at 1100°C for 100 h (Fisher et al., 2008a)

During growth of the single crystal in the conventional furnace, single crystal growth, matrix grain growth and matrix densification take place simultaneously. During crystal growth, pores in the matrix can be picked up by the moving single crystal/matrix interface. If the pores then separate from the interface, they will become trapped in the single crystal. The size of the trapped pores increases with crystal growth distance. This is probably due to pore coalescence in the matrix before the crystal/matrix interface reaches them. Application of an external pressure during crystal growth has two benefits. Firstly, during the first stage (975°C/50 MPa for 2 h), the polycrystalline matrix is densified. Application of an external pressure promotes densification without promoting grain growth (Chiang et al., 1997). The sintering temperature can therefore be reduced, allowing the matrix to be densified without much grain growth or single crystal growth. Growing the single crystal in an already dense matrix increases the density of the crystal (Fisher et al., 2007a). Secondly, during the second stage (1100°C/50 MPa for 100 h), the $K_4CuNb_8O_{23}$ liquid phase sintering aid melts and penetrates the grain boundaries, leaving behind pores which must be eliminated. The applied pressure increases the driving force for shrinkage of these pores within the matrix and also of pores that become trapped within the crystal (Kang and Yoon, 1989).

4.3 Effect of sintering aid on crystal growth and composition

The effect of the amount of sintering aid on single crystal growth, matrix grain growth and single crystal composition was investigated (Fisher et al., 2008b). Single crystals were grown from $(K_{0.5}Na_{0.5})NbO_3$ powders with additions of 0, 0.5 and 2 mol % $K_4CuNb_8O_{23}$, using <001>-oriented $KTaO_3$ seed crystals. Before the crystal growth experiments, samples were pre-densified by hot-pressing at 975°C / 50 MPa for 2 h. Crystals were then grown in air under atmospheric pressure at 1100°C for 1-20 h.

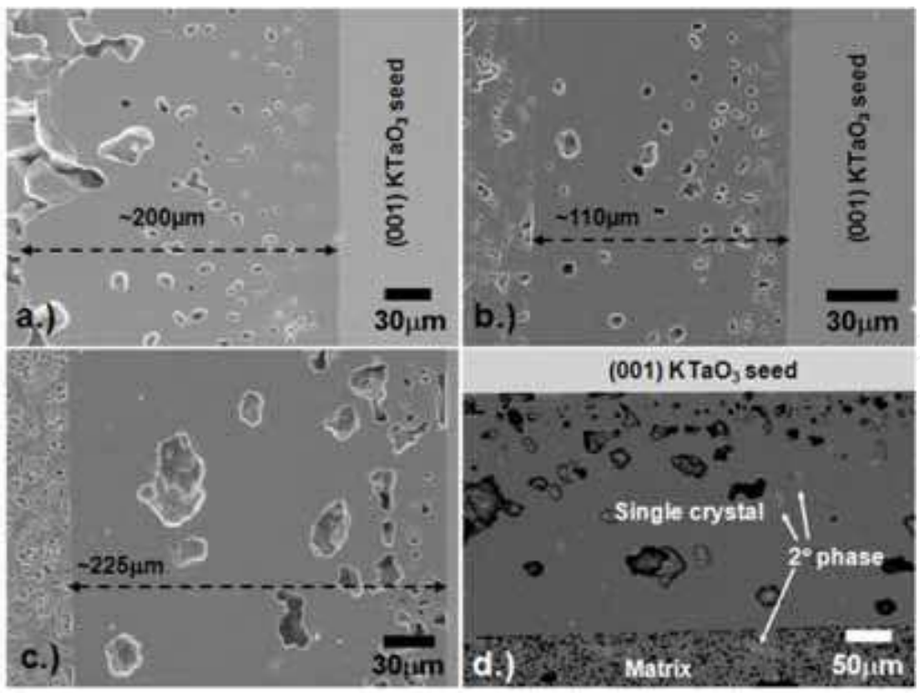

Fig. 6. Single crystals grown from $(K_{0.5}Na_{0.5})NbO_3$ powders with additions of (a) 0, (b) 0.5 and (c) 2 mol % $K_4CuNb_8O_{23}$. Crystals were grown at 1100°C for 10 h. (d) Backscattered electron image of crystal shown in Fig.6 (c) (Fisher et al., 2008b)

Secondary electron SEM images of crystals which had been grown at 1100°C for 10 h are shown in Fig.6 (a) – (c). In the sample with 0 mol % $K_4CuNb_8O_{23}$, the crystal/matrix interface is very irregular. Addition of 0.5 mol % $K_4CuNb_8O_{23}$ causes the interface to become regular but reduces the single crystal growth distance. Addition of 2 mol % $K_4CuNb_8O_{23}$ causes the crystal growth distance to increase again. Fig.6 (d) is a backscattered electron image of the sample with 2 mol % $K_4CuNb_8O_{23}$. It can be seen that there is a second phase trapped within the crystal. EDXS analysis revealed this phase to be the $K_4CuNb_8O_{23}$ sintering aid. This phase was not present within the crystals grown from samples with 0.5 mol % $K_4CuNb_8O_{23}$.

Fig.7 shows the growth distance of the single crystals and mean matrix grain sizes vs. growth time. For the samples with 0 and 0.5 mol % $K_4CuNb_8O_{23}$, crystal growth is initially rapid but tails off with growth time (Fig.7a). Addition of 0.5 mol % $K_4CuNb_8O_{23}$ causes a reduction in single crystal growth distance at all annealing times. For the sample with 2 mol % $K_4CuNb_8O_{23}$, the crystal growth rate decreases after 1 hour and then remains approximately constant up to 20 h. For the samples with 0 and 0.5 mol % $K_4CuNb_8O_{23}$, matrix grain growth is initially rapid but then tails off with annealing time (Fig.7b). For the samples with 2 mol % $K_4CuNb_8O_{23}$, after initial growth for 1 h, the matrix grain size remains almost constant up to 20 h.

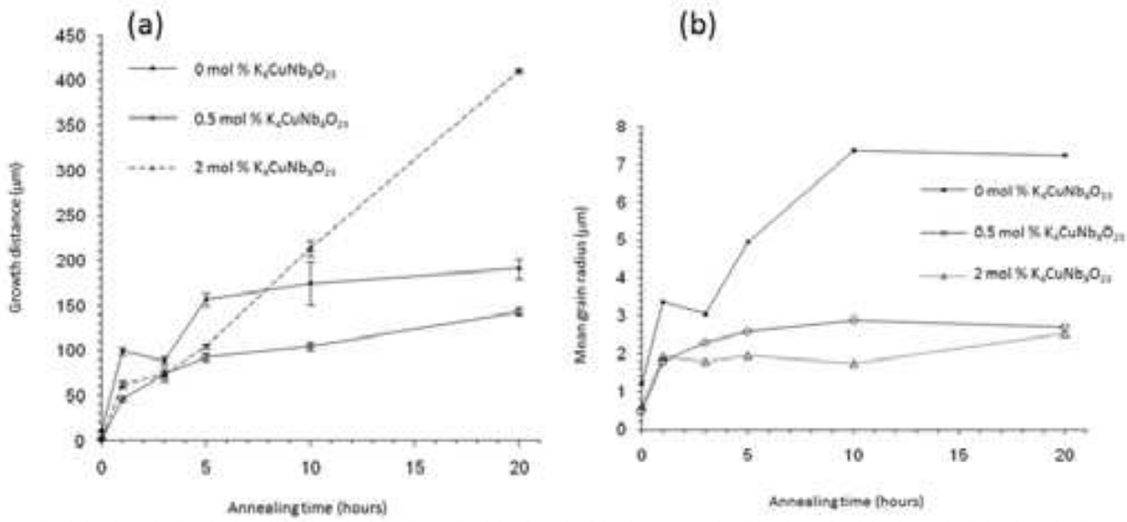

Fig. 7. (a) growth distance of single crystal and (b) mean matrix grain radius vs. growth time at 1100°C (Fisher et al., 2008b)

This behaviour is explained by considering the effect of the liquid phase on both single crystal growth and matrix grain growth. Because the seed crystal acts as a very large grain, for the single crystal equation [2] can be approximated to:

$$\Delta\mu = 2Y_{sl}\Omega\left(\frac{1}{r}\right) \tag{5}$$

Therefore, the single crystal growth rate is inversely proportional to the mean matrix grain size. In the samples with 0 and 0.5 mol % $K_4CuNb_8O_{23}$, matrix grain growth causes the driving force for single crystal growth to decrease with annealing time and the single crystal

growth rate to slow down. Addition of 0.5 mol % $K_4CuNb_8O_{23}$ liquid phase sintering aid can further reduce both the crystal and matrix grain growth rates, as the thickness of the solid/liquid interface across which atoms must diffuse increases (Kang, 2005). With addition of 2 mol % $K_4CuNb_8O_{23}$, matrix grain growth effectively ceases after 1 h. This means that the driving for single crystal growth remains constant after 1 h, allowing the crystal to keep growing even for extended annealing times.

Table 1 gives EDXS analyses of single crystals and matrix grains of samples with different amounts of $K_4CuNb_8O_{23}$. Again, single crystals of $KNbO_3$ and $NaNbO_3$ were used as standards. For the samples with 0 and 0.5 mol % $K_4CuNb_8O_{23}$, both the single crystal and matrix grains have compositions close to the nominal composition. For the sample with 2 mol % $K_4CuNb_8O_{23}$, the matrix grains have the nominal composition but the single crystal is Na-rich. According to the $KNbO_3$-$NaNbO_3$ phase diagram, $(K_{0.5}Na_{0.5})NbO_3$ at 1100°C lies just below the solidus line (Jaffe et al., 1971). It is possible that addition of 2 mol % $K_4CuNb_8O_{23}$ lowered the solidus temperature to below 1100°C. This would then cause the equilibrium solid phase to be Na-rich. Indeed, the growing single crystal is Na-rich. The matrix grains retain their original composition as their growth rate is very slow. Therefore, care must be taken when adding a liquid phase sintering aid to promote single crystal growth in this system.

Amount of $K_4CuNb_8O_{23}$ (mol %)	**K (at. %)**	**Na (at. %)**	**K/Na ratio**
0 (single crystal)	10.34 ± 0.58	10.82 ± 0.64	0.96 ± 0.04
0 (matrix)	10.64 ± 0.62	10.53 ± 0.58	1.01 ± 0.05
0.5 (single crystal)	10.41 ± 0.44	10.39 ± 0.41	0.99 ± 0.05
0.5 (matrix)	10.48 ± 0.63	10.42 ± 0.96	1.02 ± 0.13
2 (single crystal)	8.46 ± 0.54	13.35 ± 0.65	0.64 ± 0.06
2 (matrix)	10.58 ± 0.32	10.79 ± 0.99	0.99 ± 0.10
Nominal composition for $(K_{0.5}Na_{0.5})NbO_3$	10	10	1

Table 1. EDXS analyses of single crystals and matrix grains of samples annealed at 1100°C for 10 h (Fisher et al., 2008b).

4.4 Growth of $[(K_{0.5}Na_{0.5})_{0.97}Li_{0.03}](Nb_{0.8}Ta_{0.2})O_3$ single crystals by SSCG.

The SSCG method was successfully applied to the growth of (Li, Ta)-KNN modified single crystals (Fisher et al., 2007b). Powder of a nominal $[(K_{0.5}Na_{0.5})_{0.97}Li_{0.03}](Nb_{0.8}Ta_{0.2})O_3$ composition was prepared in a similar way as before, but with a higher calcination temperature of 900°C. 0.5 mol % of $K_4CuNb_8O_{23}$ was added as a liquid phase sintering aid. A <001>-oriented $KTaO_3$ single crystal was used as a seed. The sample was pre-densified by hot pressing at 975°C / 50 MPa for 2 h. The crystal was grown by annealing in air at 1135°C for 50 hours under atmospheric pressure. A single crystal ~100µm thick grew on the seed (Fig.8). SEM-EDXS analysis showed that the single crystal and the matrix grains have the same composition; however, it was not possible to analyse Li content by means of EDXS.

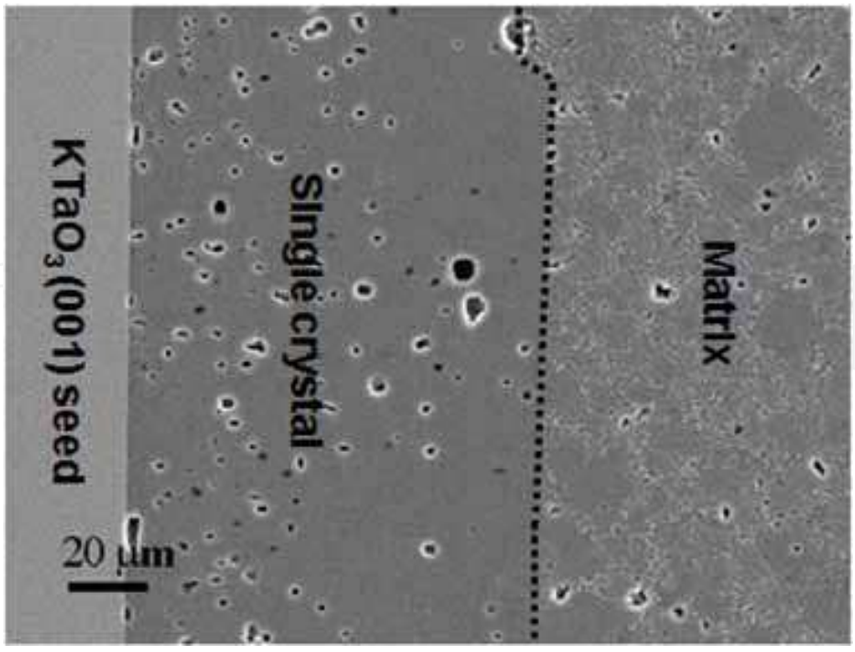

Fig. 8. SEM micrograph of $[(K_{0.5}Na_{0.5})_{0.97}Li_{0.03}](Nb_{0.8}Ta_{0.2})O_3$ Single Crystal grown by SSCG (Fisher et al., 2007b)

5. Dedicated structural and compositional study of a $(K_{0.5}Na_{0.5})NbO_3$ single crystal

The studies of structure and composition were performed on the hot-pressed KNN single crystals (see Fig. 5a). For the single crystal XRD setup, the size of the single crystals after their removal from the matrix was not sufficient. Therefore, the obtained crystals were crushed and a powder XRD setup was used.

In Fig. 9, experimental XRD powder diffraction patterns of the crushed KNN single crystal and a polycrystalline KNN ceramic, as well as calculated a XRD diffraction pattern are shown. The inset in Fig. 9 shows an enlarged view of the 100/001 and 010 diffraction peaks for the KNN single crystal and ceramic. Both the single crystal and ceramic have narrow and well defined peaks. No secondary phases were detected (Benčan et al., 2009). In previous work, different workers have refined KNN unit cell parameters using perovskite unit cells with orthorhombic symmetry (Attia et. al., 2005), monoclinic symmetry (Shiratori et. al., 2005) and also triclinic symmetry (Shiratori et. al., 2005). Our experimental data was fitted using the monoclinic symmetry given by Tellier et al. (Tellier et al. 2009), with unit cell parameters a=4.0046Å, b=3.9446 Å, c=4.0020 Å, and β=90.3327°.

A precise chemical analysis of the KNN single crystal was performed by WDXS and semi-quantitative EDXS analysis in the SEM at twelve selected points across the KNN single crystal. For WDXS analysis, $KNbO_3$ and $NaNbO_3$ single crystals were used as standards. Table 2 shows the determined elemental composition of the KNN single crystal, which is very close to the nominal one. The small variations in the values of standard deviation for both WDXS and EDXS analysis serve as proof of the crystal's homogeneity. The latter makes it possible to use these crystals as reference standards for the quantitative analysis of sodium and potassium in other materials (Benčan et al., 2009).

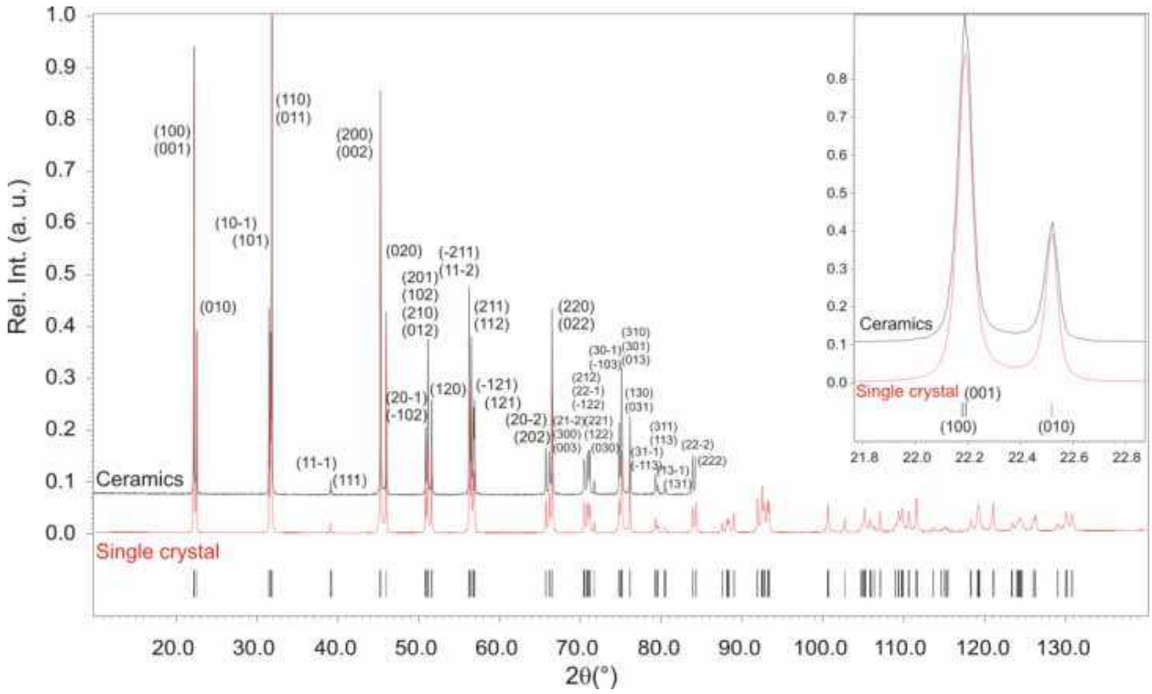

Fig. 9. XRD powder diffraction patterns of the crushed KNN single crystal and polycrystalline KNN ceramic. A calculated XRD pattern using a monoclinic KNN unit cell is added (Benčan et al., 2009)

Element	Nominal composition	WDXS		EDXS	
	at%	at%	STDEV	at%	STDEV
K	10	10.06	0.08	9.5	0.1
Na	10	10.03	0.07	9.8	0.2
Nb	20	19.89	0.10	20.3	0.3
O	60	60.02	0.15	60.4*	0.5

Table 2. Elemental composition in at% of the KNN single crystal, determined by WDXS and EDXS, with standard deviation (STDEV). Nominal composition is shown for comparison. Oxygen (*) is calculated from the stoichiometry (Benčan et al., 2009)

The domain structure of KNN single crystals at micro- and nano-scales was analysed using the techniques of optical, scanning and transmission electron microscopy (Benčan et al., 2009). A polarized light optical micrograph of the KNN single crystal is shown in Fig. 10a. The crystal is still embedded in the KNN ceramic matrix. Large ferroelectric domains from 50 to 100 microns in size are revealed by dark/bright contrast oscillations in the micrograph. These large domains in turn contain smaller domains with dimensions from tens of microns down to hundreds of nm. The smaller domains have a herring bone 90° arrangement, as shown in the inset. in Fig. 10a. The larger domains in the single crystal were also probed by electron backscattered diffraction (EBSD). The EBSD image (Fig. 10b) shows the distribution of the orientations in the crystal and surrounding matrix. Differences in colour inside the single crystal are attributed to the differently oriented ferroelectric domains. From the colour-key inverse-pole-figure it can be seen that the orientation inside the single crystal is

changing by 90° and that there are three different orientations rotated to each other by 90° angles.

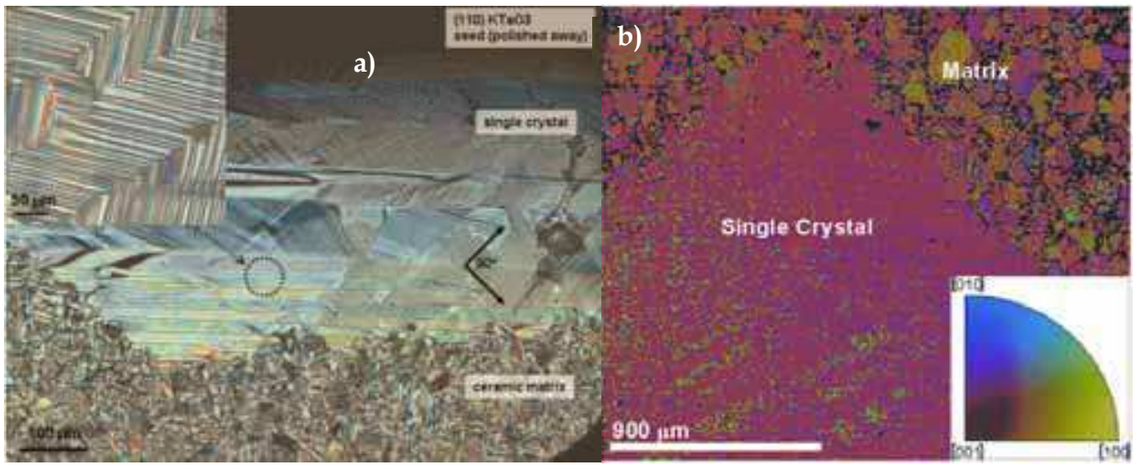

Fig. 10. Optical microscope micrographs of the KNN single crystal and its domain microstructure. The inset shows a herring bone 90° arrangement of smaller domains (a) EBSD orientation map of the KNN single crystal and the corresponding color-key inverse-pole-figure (b) (Benčan et al., 2009)

In order to determine the domain structure at the nanometer scale, the specimen was investigated by TEM (Benčan et al., 2009). Smaller saw-like domains with a size of about 50nm were arranged within the larger ones (Fig.11).

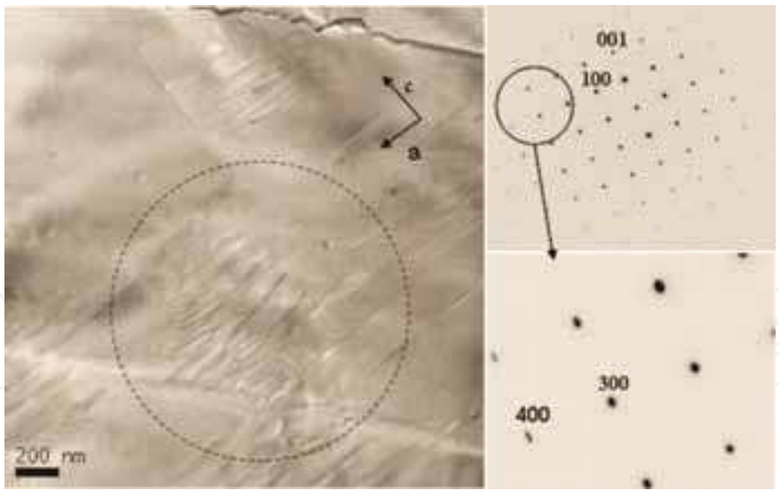

Fig. 11. TEM-BF image of the KNN single crystal with corresponding SAED patterns showing the presence of 180 ° domains. Due to the very small difference in a and c unit cell parameters, a and c axes were chosen arbitrarily (Benčan et al., 2009)

The overlapping of these domains is represented by the selected area diffraction (SAED) pattern in the [010] zone axis, taken from the area of ~1.5 µm. Splitting of the {h00} or {00l} reflections parallel to the <001> or <100> directions is seen. This is due to the β angle (~ 90.3°). Such patterns can be experimentally observed only in the case where the [100] or

[001] direction of one domain is parallel to the [-100] or [00-1] direction of the other one, meaning that these are 180° domains.

6. Dielectric, ferroelectric, piezoelectric and electrostrictive properties of $K_{0.5}Na_{0.5}NbO_3$ single crystals

The dielectric properties of a hot-pressed KNN single crystal (see Fig. 5a for reference) were measured on the as-cut piece of crystal in two perpendicular orientations. These were determined from EBSD analysis and described as [1 $\bar{3}$ 1] and the [$\overline{323}$]. Fig. 12 shows the temperature dependence of the dielectric constant (ε) and the dielectric losses (tan δ) measured for the KNN single crystal in the above mentioned directions and also for the surrounding polycrystalline KNN matrix. The highest value of ε was obtained for the [1 $\bar{3}$ 1] direction of the KNN single crystal across whole temperature range. At the same time, two phase transitions from the monoclinic to the tetragonal phase (T_1) at around 193°C, and from the tetragonal to the cubic phase (T_2) at around 410°C were measured (Ursič et al, 2010). The latter are in accordance with the transitions observed in the surrounding polycrystalline KNN ceramic, which is another indication of the obtained crystal compositional homogeneity. Table 3 summarizes the dielectric properties obtained for the KNN single crystal in both directions and for the surrounding polycrystalline KNN matrix, and gives a comparison with the dielectric properties of KNN-based single crystals reported in the literature.

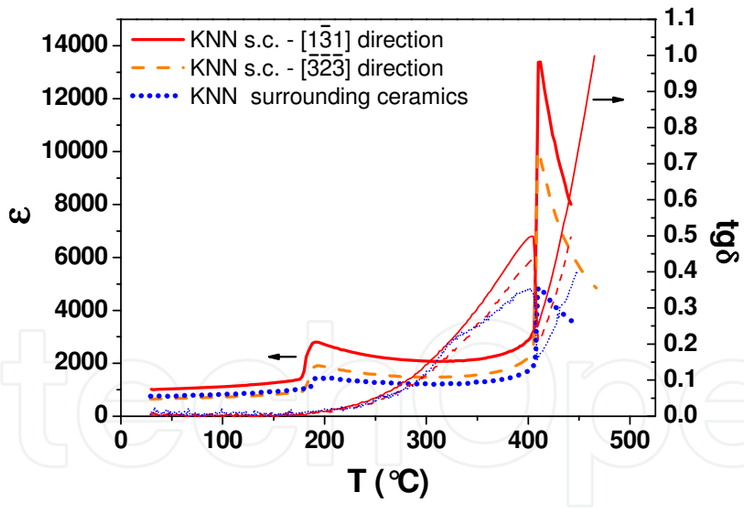

Fig. 12. Comparison of ε (thick lines) and tanδ (thin lines) as a function of the temperature for the KNN single crystal in [1 $\bar{3}$ 1] and the [$\overline{323}$] directions and for KNN surrounding ceramics measured at 100 kHz (Uršič et al., 2010).

Due to the high dielectric constant, the [1 $\bar{3}$ 1] direction of KNN single crystal was chosen for further measurements of the ferroelectric, piezoelectric and electrostrictive properties. The ferroelectric properties, i.e. the remnant polarization (Pr) and coercive field (Ec) measured for the KNN single crystal and surrounding polycrystalline KNN matrix, are compared to the literature and shown in Table 4.

System	Freq. (kHz)	ε_{Troom}	$tg\,\delta_{Troom}$	T_1 (°C)	T_2 (°C)
KNN s.c. [1 $\bar{3}$ 1] this study	100	1015	0.01	192	410
KNN s.c. [$\overline{323}$] this study	100	650	0.01	193	409
KNN ceramics this study	100	750	0.01	193	411
$K_{0.5}Na_{0.5}NbO_3$ s.c. [001] Lin et al., 2009	100	240	0.02	205	393
$K_{0.47}Na_{0.53}NbO_3$ s.c. $[100]_c$ Kizaki et al., 2007	1000	600	below 0.1	190	390
$K_{0.53}Na_{0.47}Mg_{0.004}Nb_{0.996}O_y$ s.c. $[100]_c$ Kizaki et al., 2007	1000	740	below 0.1	160	390
$0.95(K_{0.5}Na_{0.5})NbO_3$-$0.05LiNbO_3$ s.c. [001] Chen et al., 2007	100	185	0.01	192	426
$Li_{0.02}(Na_{0.5}\,K_{0.5})_{0.98}NbO_3$ s.c. $[001]_c$ Davis et al., 2007	1	205	0.33	177	/

Table 3. The ε, tgδ and monoclinic - tetragonal (T_1) and tetragonal - cubic (T_2) phase transition temperatures for KNN single crystal in the [1 $\bar{3}$ 1] and the [$\overline{323}$] directions and for KNN ceramics. For comparison the dielectric properties obtained on KNN based single crystals by different groups are added (Uršič et al., 2010)

System	Freq. (Hz)	P_r (μC/cm²)	E_c (kV/cm)
KNN s.c. [1 $\bar{3}$ 1] this study	50	17	24
KNN ceramics this study	50	15	24
$K_{0.47}Na_{0.53}NbO_3$ s.c. $[100]_c$ Kizaki et al., 2007	1	/	/
$K_{0.53}Na_{0.47}Mg_{0.004}Nb_{0.996}O_y$ s.c. $[100]_c$ Kizaki et al., 2007	1	40	12
$0.95(K_{0.5}Na_{0.5})NbO_3$-$0.05LiNbO_3$ s.c. [001] Chen et al., 2007	10	9	22

Table 4. Ferroelectric properties of KNN single crystalsin the [1 $\bar{3}$ 1] direction and for KNN ceramics. For comparison the ferroelectric properties obtained on KNN based single crystals by different groups are added (Uršič et al., 2010)

The displacement signal versus the applied voltage of the KNN single crystal in the [1 $\bar{3}$ 1] direction and of the surrounding KNN ceramic were measured using an atomic force microscope (AFM). Prior to the analysis, an AFM measurement was performed as a reference on glass under the same experimental conditions as used for the KNN single crystal and ceramics. No strain was observed for the non-piezoelectric glass, confirming that strains observed during AFM analysis of the KNN crystal and ceramics are piezoelectric in nature. The KNN single crystals were not poled before the AFM measurement.
The obtained displacement signal consists of two components. The first component has the same frequency as the applied voltage, i.e., this is the linear piezoelectric component (see Fig. 13). The second component is the pronounced quadratic component with the double frequency (see inset in Fig. 14). The piezoelectric coefficients d_{33}, shown in Fig. 13, were determined from the slopes of the linear fits of the linear component of displacement versus the applied voltage (Uršič et al., 2010).
The d_{33} piezoelectric coefficients for the KNN single crystal and for the surrounding ceramic are approximately 80 pm/V at a measurement frequency of 2 Hz. As frequency increases,

the d_{33} value for the KNN single crystal decreases (see Fig.13). Although very small applied electric fields (up to 0.1 kV/mm) were used to measure the piezoelectric coefficient for the KNN single crystal, the obtained d_{33} value (80 pm/V) was in the same range as for the poled KNN ceramic. The explanation of such behaviour can be given by the domain structure of the KNN single crystal. As shown in Section 5 the KNN single crystal consists of large 90° domains with widths of up to 100 microns, and smaller 180° domains with widths ranging between a few tens of nms to 300 nm. Since the contact area of the AFM tip is around 20 nm, it is likely that only the smaller 180° domain walls are moving during the AFM measurements. These small 180° domains probably contribute to the obtained linear response of the KNN single crystal. The inability of the 180° domains to reorientate quickly enough at higher frequencies explains the decrease in d_{33} with increasing measurement frequency. It has been previously demonstrated by McKinstry et al. (McKinstry et al., 2006) that if the mobility of 90° domains is limited, then the 180° domains can contribute to the piezoelectric linear response.

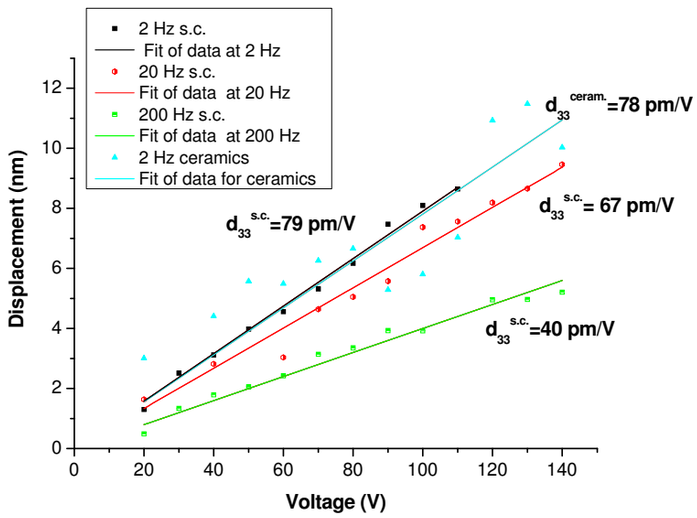

Fig. 13. The linear part of displacement versus voltage amplitude of KNN single crystal in [1 $\bar{3}$ 1] direction measured at 2 Hz, 20 Hz and 200 Hz. The measurement for KNN surrounding ceramics at 2 Hz is added for comparison (Uršič et al., 2010)

The electrostrictive coefficients (M_{33}) were determined from the slope of the linear fit of the relative strain versus the square of the amplitude of the electric field, as shown in Fig. 14. The M_{33} for the surrounding KNN ceramic was lower than that of the KNN single crystal.
The measured values M_{33} for the KNN single crystal are significantly higher than values of M_{33} for PMN-based single crystals. The highest obtained electrostrictive coefficient for a $0.65Pb(Mg_{1/3}Nb_{2/3})O_3$-$0.35PbTiO_3$ single crystal was in the range 1.3 to $4x10^{-15}$ m^2/V^2 at 0.01 Hz; a 90° domain wall contribution to electrostriction was reported (Bokov&Ye, 2002). Such a high M_{33} value for the KNN single crystal can arise from the intrinsic electrostrictive behaviour as well as the extrinsic contribution, i.e., the strain from the domain-wall motion. Most probably in the KNN single crystal, the main contribution to electrostrictive strain arises from the contribution of 180° domain walls. Our results agree with the findings obtained by McKinstry et al. (McKinstry et al., 2006), who showed that 180° domains walls

can contribute to the linear response as well as to electrostrictive strain response in ferroelectric materials. Although the pure electrostrictive response should be frequency independent, they observed in (111) $Pb(Zr_{0.45}Ti_{0.55})O_3$ thin films a decrease of the second-order strain with frequency by 20%, as was also the case for our KNN single crystal.

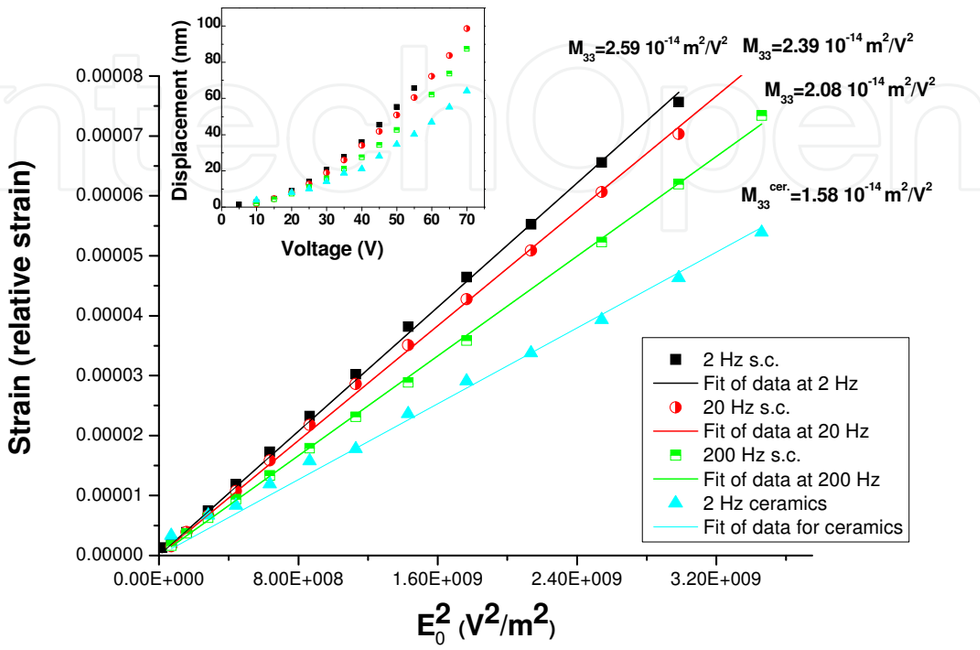

Fig. 14. Relative strain versus square of the amplitude of the electric field of KNN single crystal in the [1 $\bar{3}$ 1] direction at 2 Hz, 20 Hz and 200 Hz. Inset shows the quadratic part of displacement versus voltage for KNN single crystal. The measurement for KNN surrounding ceramics at 2 Hz is added for comparison (Uršič et al., 2010)

7. Conclusions

In this chapter the principles of the SSCG technique and its application to the growth of $K_{0.5}Na_{0.5}NbO_3$ (KNN) and Li,Ta-modified KNN single crystals were presented. With the use of the complementary analytical characterization techniques, i.e. XRD, optical microscopy and electron microscopy (SEM, EDXS, WDXS, EBSD, TEM, SAED), the precise compositional and structural analysis of KNN single crystals was performed and the correlation with its electrical properties was given.

There are several possible directions for future work. First, it would be useful to grow larger single crystals. This will enable crystals to be cut in controlled orientations e.g along the [001] or [110] directions and their properties measured and compared with KNN crystals grown by solution-based methods. Furthermore, alternative seed crystals need to be found. Although $KTaO_3$ single crystals make excellent seeds, they are rather expensive and to grow large single crystals, large seed crystals are needed. If cheaper alternatives could be found, this would reduce the cost of growing large KNN single crystals. Work needs to be done in growing single crystals from seeds placed on top of the ceramic substrate. Finally, growth of other compositions such as Li-doped KNN should be carried out.

8. Acknowledgments

Dr. Daniel Rytz, from FEE GmbH, Germany is acknowledged for the preparation of $KTaO_3$ seeds. The authors wish to acknowledge the financial support of the Slovenian Research Agency (P2-105) and the 6FP project IMMEDIATE.

9. References

Arndt, U.W. & Willis, B.T.M. (1966).*Single Crystal Diffractometry* (1st edition), Cambridge University Press, ISBN:978-0-521-04060-0, New York

Attia, J., Bellaiche, M., Gemeiner, P., Dkhil, B. & Malič, B. (2005). Study of potassium-sodium-niobate alloys: A combined experimental and theoretical approach. *Journal de Physique IV* (*Proceedings)*, Vol. 128, No.1, (September 2005), pp. 55–60, ISSN:1155-4339

Bauser, E. & Strunk, H. (1982).Dislocations as Growth Step Sources in Solution Growth and Their Influence on Interface Structure.*Thin Solid Films*, Vol. 93, Nos. 1-2, (July 1982), pp. 185-94,ISSN:0040-6090

Benčan, A., Tchernychova, E., Godec, M., Fisher, J. & Kosec M. (2009).Compositional and Structural Study of a $(K_{0.5}Na_{0.5})NbO_3$ Single Crystal Prepared by Solid State Crystal Growth. *Microscopy and Microanalysis*, Vol.15, No.5, (October 2009), pp. 435-440, ISSN:1431-9276

Benčan, A., Tchernychova, E., Šturm, S., Samardzija, Z., Malič, B. & Kosec, M. (2011). Approches for a reliable compositional analysis of alkaline-based lead-free perovskite ceramics using microanalytical methods. *Journal of Advanced Dielectrics*,Vol.1, No.1, (January 2011), pp. 41-52, ISSN:2010-1368

Bennema P. (1993). Growth and Morphology of Crystals. In:*Handbook of Crystal Growth 1 Fundamentals Part A: Thermodynamics and Kinetics*, D. T. J. Hurle (Ed.), pp. 481–581,ISBN: 0444889086, North-Holland, Amsterdam

Bokov, A. & Ye, Z. G. (2002). Giant electrostriction and stretched exponential electromechanical relaxation in $0.65Pb(Mg_{1/3}Nb_{2/3})O_3$-$0.35PbTiO_3$ crystals, *Journal of Applied Physics*, Vol. 91,No. 10 (May 2002),pp. 6656- 6661, ISSN:0021-8979

Bomlai, P.,Wichianrat, P.,Muensit, S. & Milne, S.J. (2007). Effect of Calcination Conditions and Excess Alkali Carbonate on the Phase Formation and Particle Morphology of $Na_{0.5}K_{0.5}NbO_3$ Powders. *Journal of American Ceramic Society*,Vol. 90, No. 5, (May 2007),pp. 1650-1655, ISSN:0002-7820

Burton, W. K., Cabrera, N. & Frank, F. C. (1951). The Growth of Crystals and the Equilibrium Structure of Their Surfaces. *Philosophical Transactions of the Royal Society of London Series A*, Vol. 243, (June 1951), pp.299-358, ISSN: 0962-8428

Chen, K., Xu, G., Yang, D. ,Wang, X. & Li J. (2007). Dielectric and piezoelectric properties of lead-free $0.95(K_{0.5}Na_{0.5})NbO_3$–$0.05LiNbO_3$ crystals grown by the Bridgman method. *Journal of Applied Physics*,Vol. 101,No. 4, (February 2007), pp. 0441031-4,ISSN:0021-8979

Chiang, Y. M., Birnie III, D. & Kingery, W. D. (1997). *Physical Ceramics: Principles for Ceramic Science and Engineering*, John Wiley & Sons, Inc., ISBN 0-471-59873-9, New York

Choi, J.J., Ryu, J. & Kim, H. E. (2001). Microstructural Evolution of Transparent PLZT Ceramics Sintered in Air and Oxygen Atmospheres. *Journal of the American Ceramic Societ*,.Vol. 84, No. 7 (July 2001), pp. 1465-1469, ISSN:0002-7820

Davis, M., Klein, N.,Damjanovič, D. & Setter, N. (2007). Large and stable thickness coupling coefficients of $[001]_c$ oriented $KNbO_3$ and Li-modified $(K,Na)NbO_3$ single crystals. *Applied Physics Letters*.Vol. 90, No. 6 (February 2007), pp.062904 1-3,ISSN:0003-6951

DeVries.R.C. (1964). Growth of Single Crystals of $BaTiO_3$ by Exaggerated Grain Growth.*Journal of the American Ceramic Society*, Vol. 47, No. 3 (March 1964), pp. 134-136,ISSN:0002-7820

Fisher, J. G., Benčan, A., Holc, J., Kosec, M., Vernay, S. & Rytz, D. (2007a). Growth of Potassium Sodium Niobate Single Crystals by Solid State Crystal Growth. *Journal of Crystal Growth*, Vol. 303, No. 2 (May, 2007), pp. 487-492, ISSN:0022-0248

Fisher, J. G., Benčan, A., Bernard, J., Holc, J., Kosec, M., Vernay, S. & Rytz, D. (2007b). Growth of $(Na,K,Li)(Nb,Ta)O_3$ Single Crystals by Solid State Crystal Growth. *Journal of the European Ceramic Society*, Vol. 27, Nos. 13-15 (2007), pp. 4103-4106,ISSN:0955-2219

Fisher, J. G., Benčan, A., Kosec, M., Vernay, S. & Rytz, D. (2008a).Growth of Dense Single Crystals of Potassium Sodium niobate by a Combination of Solid-State Crystal Growth and Hot Pressing. *Journal of the American Ceramic Society*, Vol. 91, No. 5 (May 2008), pp. 1503-1507,ISSN:0002-7820

Fisher, J. G., Benčan, A., Godnjavec, J. & Kosec, M. (2008b). Growth Behaviour of Potassium Sodium Niobate Single Crystals Grown by Solid-State Crystal Growth Using $K_4CuNb_8O_{23}$ as a Sintering Aid. *Journal of the European Ceramic Society*, Vol. 28, No. 8 (2008), pp. 1657-1663,ISSN:0955-2219

Goldstein, J., Lyman, C.E., Newbury, D.E.,Lifshin, E., Echlin, P., Sawyer, L., Joy D.C. & Michael, J.R. (2003). *Scanning Electron Microscopy and X-Ray Microanalysis*, (3rd edition), Kluwer Academic and Plenum Publishers, ISBN:0-306-47292-9, New York

Gorzkowski, E. P., Chan, H. M. & Harmer, M. P. Effect of PbO on the Kinetics of {001} $Pb(Mg_{1/3}Nb_{2/3})O_3$- 35mol%$PbTiO_3$ Single Crystals Grown into Fully Dense Matrices. *Journal of the American Ceramic Society*, Vol.89, No.3, (March 2006) pp. 856-862,ISSN:0002-7820

Greenwood, G. W. (1956). The Growth of Dispersed Precipitates in Solutions. *ActaMetallurgica*,Vol. 4, No. 3 (May 1956), pp. 243-348, ISSN:0001-6160

Hennings, D. F. K., Janssen, R. & Reynen, P. J. L. (1987). Control of Liquid-Phase- Enhanced Discontinuous Grain Growth in Barium Titanate. *Journal of the American Ceramic Society*, Vol. 70, No. 1 (January 1987), pp.23-27,ISSN:0002-7820

Hirth, J. P. & Pound, G.M. (1963). Condensation and Evaporation. *Progress in Materials Science*.Vol. 11, (1963), pp. 17-192,ISSN:0079-6425

Jaffe, B., Cook Jr., W. R. & Jaffe, H. (1971). Perovskite niobates and tantalates and other ferroelectric and antiferroelectric perovskites, In: *Piezoelectric Ceramics*, Eds. J.P.Roberts & P.Popper, Academic Press, pp. 185-212, ISBN 0123795508, London

Jenko, D., Benčan, A., Malič, B., Holc, J. & Kosec, M. (2005). Electron microscopy studies of potassium sodium niobate ceramics. *Microscopy and microanalysis*, Vol. 11, No.6 (December 2005), pp. 572-580, ISSN:1435-8115

Kang, S. J. L. & Yoon, K. J. (1989). Densification of Ceramics Containing Entrapped Gases. *Journal of the European Ceramic Society*, Vol. 5, No. 2 (1989), pp. 135-139, ISSN:0955-2219

Kang, S. J. L. (2005). Chapter 15, Grain Shape and Grain Growth in a Liquid Matrix, In: *Sintering: Densification, Grain Growth and Microstructure*, pp. 205-26, Elsevier, ISBN:07506 63855, Oxford

Khan, A., Meschke, F. A., Li, T., Scotch, A. M., Chan, H. M. & Harmer, M. P. (1999). Growth of $Pb(Mg_{1/3}Pb_{2/3})O_3$ – 35 mol% $PbTiO_3$ Single Crystals from (111) Substrates by

Seeded Polycrystal Conversion.*Journal of the American Ceramic Society*,Vol. 82, No.11, (November 1999), pp. 2958-62,ISSN:0002-7820

Kim, M. S., Fisher, J. G., Kang, S. J. L. & Lee, H. Y. (2006). Grain Growth Control and Solid-State Crystal Growth by Li_2O/PbO Addition and Dislocation Introduction in the PMN-35 PT System. *Journal of the American Ceramic Society*, Vol. 89, No. 4 (April 2006), pp. 1237–1243,ISSN:0002-7820

Kizaki, Y., Noguchi, Y. & Miyayama, M. (2007). Defect control for Superior Properties in $K_{0.5}Na_{0.5}NbO_3$ Single Crystals. *Key Engineering Materials*, Vol. 350, (October 2007), pp. 85-88, ISSN:1013-9826

Kosec, M., Malič, B., Benčan, A. & Rojac, T. (2008). KNN-based piezoelectric ceramics. In:*Piezoelectric and Acoustic Materials for Transducer Applications*,Eds.: A. Safari and E. K. Akdogan,pp. 81-102, Springer, ISBN: 978-0-387-76538-9., New York

Kosec, M., Malič, B., Benčan, A., Rojac, T. & Tellier, J. (2010). Alkaline niobate-based piezoceramics: crystal structure, synthesis, sintering and microstructure. *Functional materials letters* Vol. 3, No.1, (March 2010), pp. 15-18, ISSN:1793-6047

Kosec, M. &Kolar, D. (1975).On Activated Sintering and Electrical Properties of $NaKNbO_3$. *Material Research Bulletin*, Vol. 10, No. 5, (May 1975), pp. 335–40,ISSN: 0025-5408

Kugimiya, K., Hirota, K. & Matsuyama, K. (1990). Process for Producing Single Crystal Ceramics. US Pat. No. 4900393, 1990.

Kwon, S. K., Hong, S. H., Kim, D. Y. & Hwang, N. M. (2000). Coarsening Behavior of Tricalcium Silicate (C_3S) and Dicalcium Silicate (C_2S) Grains Dispersed in a Clinker Melt. *Journal of the American Ceramic Society*, Vol. 83, No. 5, (May 2000), pp. 1247-1252,ISSN:0002-7820

Lee, B. K., Chung, S. Y. & Kang, S. J. L. (2000). Grain Boundary Faceting and Abnormal Grain Growth in $BaTiO_3$. *Acta Materialia*, Vol. 48, No. 7, (April 2000), pp. 1575-1580ISSN:1359-6454

Lee H. Y. (2003). Solid-State Single Crystal Growth (SSCG) Method: A Cost-effective Way of Growing Piezoelectric Single Crystals. In: P*iezoelectric Single Crystals and their Applications*, S. Trolier-McKinstry, L. E. Cross and Y. Yamashita (Eds.), pp. 160-177, Pennsylvania State University, State College, PA

Lin, D., Li, Z., Zhang, S., Xu Z. & Yao, X. (2009). Dielectric/piezoelectric properties and temperature dependence of domain structure evolution in lead free $K_{0.5}Na_{0.5}/NbO_3$ single crystal. Solid State Communications, Vol. 149, No.39-40, (October 2009), pp. 1646- 1649, ISSN:0038-1098

Malič, B., Benčan, A., Rojac, T. & Kosec, M. (2008a). Lead-free Piezoelectrics Based on Alkaline Niobates: Synthesis, Sintering and Microstructure. *Acta Chimica Slovenica*, Vol. 55, No.4, (December 2008),pp. 709-718, ISSN: 1318-0207

Malič, B., Jenko, D., Holc, J., Hrovat, M. & Kosec, M. (2008b). Synthesis of sodium potassium niobate: a diffusion couples study. *Journal of the American Ceramic Society*, Vol. 91, No.6, pp. 1916-1922, ISSN: 0002-7820

Matsubara, M., Yamaguchi, T., Sakamoto, W., Kikuta K., Yogo, T. & Hirano, S. I. (2005). Processing and Piezoelectric Properties of Lead-Free (K,Na)(Nb,Ta)O_3 Ceramics. *Journal of the American Ceramic Society*, Vol. 88, No. 5, (May 2005), pp. 1190-1196,ISSN:0002-7820

McKinstry, T. S., Gharb N. B. & Damjanovic, D. (2006). Piezoelectric nonlinearity due to motion of 180°domain walls at subcoercive fields: A dynamic poling model. *Applied Physics Letters*, Vol. 88, No.20, (May 2006) pp. 202901-3, ISSN:0003-6951

Park, S.E. & Shrout, T.R. (1997). Ultrahigh strain and piezoelectric behavior in relaxor based ferroelectric single crystals. *Journal of Applied Physics*, Vol. 82, No.4, (August 1997) pp. 1804-1811,ISSN:0021-8979

Rehrig, P. W., Park, S. E., Trolier-McKinstry, S., Messing, G. L., Jones, B. & Shrout, T. R.(1999). Piezoelectric Properties of Zirconium-doped Barium Tiotanate Single Crystals Grown by Templated Grain Growth. *Journal of Applied Physics*, Vol. 86, No.3 (August 1999), pp. 1657-1661, ISSN:0021-8979

Rödel, J., Jo, W., Seifert, K., Anton, E. M., Granzow, T. & Damjanovič, D. (2009). Perspective on the Development of Lead-free Piezoceramics, *Journal of the American Ceramic Soc*iety, Vol. 92, No.6, (June 2009), pp. 1153- 1177, ISSN:0002-7820

Saito, Y., Takao, H., Tani, T., Nonoyama, T., Takatori, K., Homma, T., Nagaya, T. & Nakamura, M., (2004). Lead-free piezoceramics, *Nature*, Vol. 432, No. 7013, pp. 84-87 (November 2004), ISSN: 0028-0836

Samardžija, Z., Bernik, S., Marinenko, R. B., Malič, B. & Čeh, M. (2004). An EPMA Study on $KNbO_3$ and $NaNbO_3$ Single Crystals–Potential Reference Materials for Quantitative Microanalysis. *Microchimica Acta*, Vol. 145, Nos. 1-4, (2004), pp. 203–208, ISSN:0026-3672

Seo, C. E. & Yoon, D. Y. (2005).The Effect of MgO Addition on Grain Growth in PMN-35PT.*Journal of the American Ceramic Society*, Vol. 88, No. 4, (April 2005), pp. 963-967, ISSN:0002-7820

Shiratori, Y., Magrez, A. & Pithan C. (2005). Particle Size Effect on the Crystal Structure Symmetry of $K_{0.5}Na_{0.5}NbO_3$. *Journal of the European Ceramic Society*, Vol. 25, No. 12 (2005), pp. 2075-2079, ISSN:0955-2219

Tellier, J., Malič, B., Dkhil, B., Jenko, D., Cilensek, J. & Kosec, M. (2009). Crystal structure and phase transition of sodium potassium niobateperovskite. *Solid State Science*,Vol. 11, No. , (February 2009),pp. 320–324, ISSN:1293-2558

Uršič, H., Benčan, A., Škarabot, M., Godec, M. & Kosec, M. (2010). Dielectric, ferroelectric, piezoelectric, and electrostrictive properties of $K_{0.5}Na_{0.5}NbO_3$ single crystals. *Journal of Applied Physics*, Vol.107, No. 3, (February 2010), pp. 033705-5, ISSN:0021-8979

van der Eerden, J. P. (1993). Crystal Growth Mechanisms, In: *Handbook of Crystal Growth. 1 Fundamentals Part A: Thermodynamics and Kinetics*, D. T. J. Hurle (Ed.), pp. 311-475, North-Holland, ISBN: 2- 88074-246-3, Amsterdam

Wada, S., Muraoka, K., Kakemoto, H., Tsurumi, T. & Kumagai, H. (2004). Enhanced Piezoelectric Properties of Potassium Niobate Single Crystals by Domain Engineering. *Japanese Journal of Applied Physics*, Vol.43, No. 9B, (September 2004) pp.6692-6700, ISSN:0021-4922

Yamamoto, T. & Sakuma, T. (1994). Fabrication of Barium Titanate Single Crystals by Solid-State Grain growth.*Journal of the American Ceramic Society*, Vol. 77, No. 4, (April 1994), pp.1107-1109, ISSN:0002-7820

Yoon, D.Y., Park, C.W.& Koo, J.B. (2001).The Step Growth Hypothesis for Abnormal Grain Growth.In:*Ceramic Interfaces 2*, S.J.L. Kang (Ed.), pp. 2-21, Institute of Materials, ISBN:978 1 861251 18 3, London

Zhang, S., Lee, S. M., Kim, D. H., Lee, H. Y. & Shrout, T. R. (2007). Electromechanical Properties of PMN–PZT Piezoelectric Single Crystals NearMorphotropic Phase Boundary Compositions. *Journal of the American Ceramic Society* Vol. 90, No. 12 (December 2007), pp.3859-3862,ISSN:0002-7820

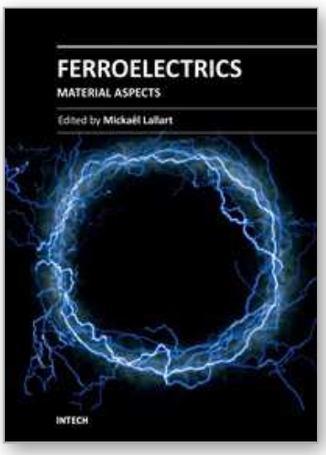

Ferroelectrics - Material Aspects
Edited by Dr. MickaÃ«l Lallart

ISBN 978-953-307-332-3
Hard cover, 518 pages
Publisher InTech
Published online 24, August, 2011
Published in print edition August, 2011

Ferroelectric materials have been and still are widely used in many applications, that have moved from sonar towards breakthrough technologies such as memories or optical devices. This book is a part of a four volume collection (covering material aspects, physical effects, characterization and modeling, and applications) and focuses on ways to obtain high-quality materials exhibiting large ferroelectric activity. The book covers the aspect of material synthesis and growth, doping and composites, lead-free devices, and thin film synthesis. The aim of this book is to provide an up-to-date review of recent scientific findings and recent advances in the field of ferroelectric materials, allowing a deep understanding of the material aspects of ferroelectricity.

InTech Europe
University Campus STeP Ri
Slavka Krautzeka 83/A
51000 Rijeka, Croatia
Phone: +385 (51) 770 447
Fax: +385 (51) 686 166
www.intechopen.com

InTech China
Unit 405, Office Block, Hotel Equatorial Shanghai
No.65, Yan An Road (West), Shanghai, 200040, China
中国上海市延安西路65号上海国际贵都大饭店办公楼405单元
Phone: +86-21-62489820
Fax: +86-21-62489821

IntechOpen